IOP Publishing | Astro Ltd
Laser Physics Letters
Laser Phys. Lett. **12** (2015) 056103 (5pp)
doi:10.1088/1612-2011/12/5/056103

Phonon modes and local polar distortions in nanoclusters of $Pb(In_{1/2}Nb_{1/2})O_3$-$Pb(Mg_{1/3}Nb_{2/3})O_3$-$PbTiO_3$ crystals probed by terahertz reflectance spectra and Raman scattering

J J Zhu[1,2], J Z Zhang[1,2], G S Xu[3], X L Zhang[1], Z G Hu[1] and J H Chu[1,2]

[1] Key Laboratory of Polar Materials and Devices, Ministry of Education, Department of Electronic Engineering, East China Normal University, Shanghai 200241, People's Republic of China
[2] National Laboratory for Infrared Physics, Shanghai Institute of Technical Physics, Chinese Academy of Science, Shanghai 200083, People's Republic of China
[3] R and D Center of Synthetic Crystals, Shanghai Institute of Ceramics, Chinese Academy of Sciences, Shanghai 201800, People's Republic of China

E-mail: zghu@ee.ecnu.edu.cn

Received 14 June 2014, revised 21 March 2015
Accepted for publication 25 March 2015
Published 20 April 2015

Abstract

Optic phonons and lattice vibrations of $Pb(In_{1/2}Nb_{1/2})O_3$-$Pb(Mg_{1/3}Nb_{2/3})O_3$-$PbTiO_3$ single crystals near the morphotropic phase boundary (MPB) are determined by terahertz (THz) reflectance spectra in a temperature range of 5.5–300 K. Raman scattering is measured with a He–Ne laser with a wavelength of 632.8 nm as the exciting source. On cooling from 300 K, the A_1 component of the splitting TO1 mode hardens, which follows the Cochran law with a critical softening temperature of 761–861 K. Moreover, the E component of the soft mode is heavily damped around 0.81 THz (27 cm^{-1}). Additional polar phonon modes, which are forbidden in the cubic structure, are activated due to the broken cubic symmetry in polar clusters.

Keywords: ferroelectric, terahertz reflectance spectra, Raman scattering, crystal, morphotropic phase boundary, soft mode

(Some figures may appear in colour only in the online journal)

1. Introduction

Piezoelectrics are of great interest for energy applications, because they can transform environmental mechanical forces into potentially useful electricity and can generate mechanical responses driven by electric forces. They are widely used in ultrasonics, energy harvesting, etc [1–6]. Ferroelectricity is mostly related to the displacement of ions, therefore there is a local separation between the center of the distribution of the positive and negative charge. The presence of disorder means that the interactions caused by displacing atoms cannot constantly induce long-range order, but can result in local ordering. For instance, in perovskite $PbTiO_3$, Pb is the twelve-fold coordinated A-site cation and Ti is the six-fold coordinated B-site cation. The Ti^{4+} ion shows a strong positive charge. Therefore, if this ion is displaced in parallel away from the center of its octahedral layer, the crystal will obtain a net polarization. The overall average ordering is conventionally revealed by x-ray or neutron diffraction, in which the Bragg peak intensities are measured and a unit cell is determined [7, 8]. Note that x-ray or neutron diffraction actually reflects an average over numerous local environments. They certainly cannot reflect the local crystal chemistry, which plays an important role in physical properties. Since the function of materials is related to their

structures, one can comprehend the origin of the properties by resolving the micro structures and electronic structures. However, local ordering in relaxor ferroelectrics persists only for a few unit cells or nanometers. Disorder, randomness and short-range order are invoked to explain many physical and chemical key properties [9]. Local order is related to the crystal chemistry of the individual ions, obviously different from the global average order revealed by conventional techniques.

As a classic example, the chemical disorder of $Pb(Mg_{1/3}Nb_{2/3})O_3$ (PMN) on the B-site results in a wide range of environments for the polar A-site atoms. Recently, $Pb(In_{1/2}Nb_{1/2})O_3$-$Pb(Mg_{1/3}Nb_{2/3})O_3$-$PbTiO_3$ (PIN-PMN-PT) ternary system with a morphotropic phase boundaries (MPB) composition was reported to have higher phase transition temperatures with similar piezoelectric properties as compared to PMN-PT, which is regarded as broadening the temperature and electric field ranges for applications [10]. The origin of large piezoelectric properties for PMN-PT based systems is polarization rotation induced by the external electric field [11, 12]. PIN-PMN-PT crystals exhibit MPB between the rhombohedral and tetragonal phases, which are thermodynamically equivalent. In the MPB region, monoclinic and/or orthorhombic phases exist that bridge the rhombohedral and tetragonal phases. Moreover, the orthorhombic/monoclinic symmetry can coexist with a rhombohedral or tetragonal phase [13, 14].

Complex dielectric properties are related to the chemical disorder of ions with different valence at the B sites. For PMN, Mg^{2+} and Nb^{5+} have the ratio of 1 : 2 at the B sites and they are short-range 1 : 1 order on a length scale of 20–50 Å. One site is occupied by Nb^{5+} and the other one by a random mixture of 1/3 Nb^{5+} and 2/3 Mg^{2+}. Terahertz (THz) and Raman spectroscopic techniques are sensitive tools for revealing the degree of B-site order [15, 16]. In contrast to the well-studied ultrahigh dielectric and piezoelectric properties, a quantitative understanding of the complex dielectric behavior in relaxors has not been fully investigated. Compared with the inelastic neutron scattering (INS), which probes couples with a relative short-wavelength comparable to the nanoclusters' size, the THz probe couples with very long-wavelength phonons, which can detect the effectively homogeneous medium averaged over the nanoclusters [17–19]. The coherent length for the THz activity determined by the range of interatomic forces is very short, which makes the local polar distortions in polar clusters observable from the THz spectra.

In this letter, we present a detailed analysis of PIN-PMN-PT on the basis of THz and Raman measurements, which provide information about the microscopic dynamics of single crystals. The results reveal several key features which are closely related to the temperature variation of the soft mode. In particular, the formation of polar clusters is manifested by splitting the polar modes from the THz spectra.

2. Experimental details

PIN-PMN-PT single crystals were grown using a vertical Bridgman technique [20]. The samples were cut perpendicular to the ⟨001⟩ direction. The nominal concentration

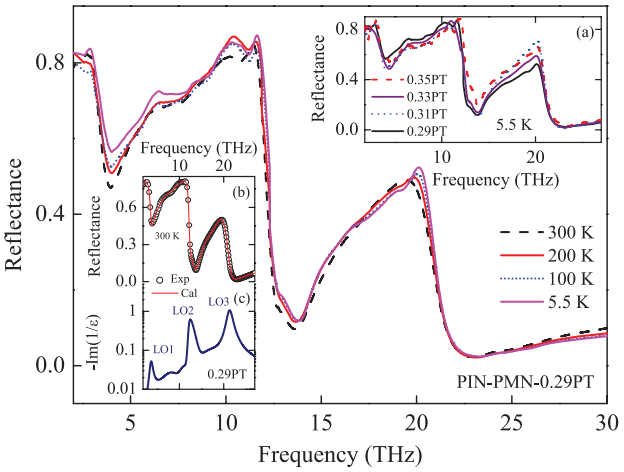

Figure 1. Temperature dependent THz reflectance spectra for PIN-PMN-0.29PT crystal. Inset (*a*) shows THz reflectance spectra of PIN-PMN-PT crystals at 5.5 K. Insets (*b*) and (*c*) show the experimental (circles) and calculated (solid line) THz reflectance spectra and -Im(1/ε) of PIN-PMN-0.29PT crystal at 300 K, respectively.

of *x*PIN-(1-*x*-*y*)PMN-*y*PT crystals was $x \sim 0.27$–0.28 and $y \sim 0.29$–0.35. The near-normal incident (~6°) THz reflectance measurements were performed from 0.75 to 30 THz using a Bruker VERTEX 80 V Fourier transform infrared spectrometer. The PIN-PMN-PT crystals were mounted into an Oxford AC-V12w continuous flow cryostat with the crystal samples in He vapor. The temperature could be varied from 5.5 to 300 K. Gold and aluminum mirrors, whose absolute reflectance was measured, were taken as references for the spectra in the high and low-frequency regions, respectively. Raman scattering measurements were carried out by using a Jobin-Yvon LabRAM HR800 UV micro-Raman spectrometer. The He–Ne laser with a wavelength of 632.8 nm was taken as the exciting source.

3. Results and discussions

The experimental and fitting THz reflectance spectra of PIN-PMN-PT crystals, taken at 5.5, 100, 200 and 300 K, are shown in figure 1. Generally, THz spectra can be fitted using the factorized oscillator model of the dielectric function:

$$\varepsilon(\nu) = \varepsilon_\infty \prod_{j=1}^{n} \frac{\nu_{\mathrm{LO}_j}^2 - \nu^2 + \mathrm{i}\nu\gamma_{\mathrm{LO}_j}}{\nu_{\mathrm{TO}_j}^2 - \nu^2 + \mathrm{i}\nu\gamma_{\mathrm{TO}_j}}. \quad (1)$$

Where the dielectric function is related to reflectance R by $R = \left|\frac{\sqrt{\varepsilon(\nu)} - 1}{\sqrt{\varepsilon(\nu)} + 1}\right|^2$. ε_∞ is the high frequency dielectric constant, ν_{TO_j} and ν_{LO_j} are the transverse optic (TO) and longitudinal optic (LO) frequency of the *j*th mode, respectively; γ_{TO_j} and γ_{LO_j} are the corresponding damping constants.

The fitting parameter values for PIN-PMN-0.29PT at 5.5 K are summarized in table 1. The frequency range above 30 THz is not shown because the reflectance pattern is almost flat and there is no phonon response. The main phonon structure was observed below 20 THz. Figure 1(*a*) shows that there is no

Table 1. Parameter values of the factorized oscillator model for PIN-PMN-0.29PT crystal are obtained by fitting THz reflectance spectra at 5.5 K.

Assignment	E (TO1)	E (TO)	A_1(TO1)	E (TO2)	A_1(TO2)	A_1(TO)	GR	E (TO3)	A_1(TO3)	GR
ν_{TO}	0.8	2.3	2.7	5.9	10.3	11.3	12	14.3	18.5	20.1
γ_{TO}	1.8	1.6	0.7	2.3	5.9	3.1	4.6	3.1	4.1	1.5
ν_{LO}	2.6	7.1	3.5	2.4	13.7	19	12.3	20.4	10.8	21.1
γ_{LO}	0.8	4.5	1.2	5.4	1.1	9.2	0.6	2.6	1.8	1.6

Note: the unit is THz and $\varepsilon_\infty = 5.43$.

obvious difference between the polar phonon structure of various PIN-PMN-PT crystals. The damping constants of some polar modes are broadening due to the rising chemical disorder in the lattice.

Three main peaks are observed in the THz spectra of PIN-PMN-PT crystals, corresponding to three infrared (IR) active phonons of a simple cubic paraelectric structure, which neglects the presence of the polar phase and four different types of ions at the B position of the ABO_3 perovskite. They are Axe-, Slater- and Last-type vibrations, respectively. The Last modes express the vibration of rigid BO_6 octahedra against Pb atoms. Two modes in the range of 4.5–10.5 THz are the so-called Slater mode, caused by the vibration of the B atoms against the O_6 octahedra. It was reported that the piezoelectric properties of PZN-PT is higher than PMN-PT because of overall lower frequencies in the Slater band of PZN-PT. The larger mass of the Zn^{2+} ion than that of the Mg^{2+} ion leads to a lower frequency of the Last-type band. However, the low frequency part of the Last band reveals a weak force constant, indicating an important Slater-type component in the frozen polarization of PZN-PT [22]. The Axe mode corresponding to the vibrations above 15 THz is mainly due to the bending of the O_6 octahedra.

The mode near 12.9 THz is IR active because the local order in the B sites leads to mutual B-atom vibrations. Similar behavior was observed in $Pb(Mg_{1/3}Nb_{2/3})O_3$-$Pb(Sc_{1/2}Nb_{1/2})O_3$-$Pb(Zn_{1/3}Nb_{2/3})O_3$ relaxors [23]. Ten polar phonons can be resolved from the THz spectra at 5.5 K. This is inconsistent with the factor group analysis for the cubic, tetragonal and rhombohedral symmetry. The cubic paraelectric perovskite structure allows three F_{1u} IR active modes and one silent mode of F_{2u} symmetry. In the case of a B-site disorder, the average primitive unit cell contains only one formula unit. In the $Fm\bar{3}m$ space group, the factor group analysis yields the following optic vibration modes: $4A_{1g}$(Raman) + E_g(Raman) + F_{1g}(-) + $4F_{1u}$(IR) + $2F_{2g}$(Raman) + F_{2u}(-). This indicates that four Raman and four IR active modes are expected in the spectra. If we assume that the crystals have a macroscopically cubic symmetry with the polar nanoregions of rhombohedral symmetry, 16 IR active modes are expected when considering the rhombohedral structure with 1 : 1 short-range order in the B site. In this case, the optic modes are $7A_1$(Raman,IR) + $2A_2$ + $9E$ (Raman,IR) and $1A_1$ + $1E$ acoustic modes. The THz probe is sensitive enough to observe the polar modes from the rhombohedral structure. Not all of them can be seen because some of them are weak or overlap with others due to their finite dampings. Note that the THz spectra shapes are similar to those of PMN, PMN-PT and other relaxors [21–24].

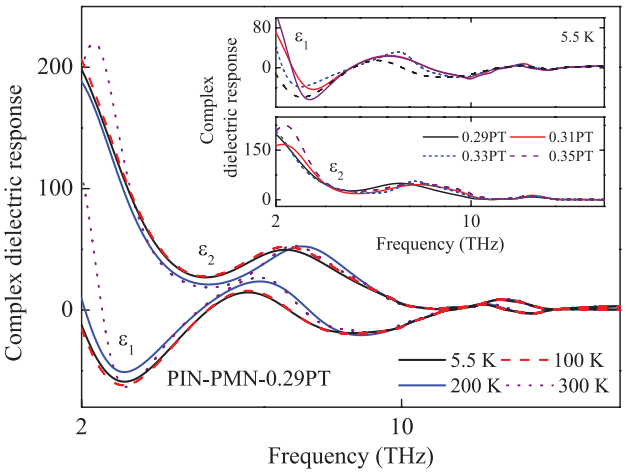

Figure 2. Complex dielectric response of PIN-PMN-0.29PT crystal obtained by fitting THz reflectance spectra at selected temperatures. The insets show the complex dielectric response of PIN-PMN-PT crystals at 5.5 K. Note that the horizontal axis is with the logarithmic unit.

The order parameter in the polar nanoregions and ferroelectric phases of Pb-based relaxors is mainly related to displacement of the Pb cation, which leads to the Last-type band at the lowest frequencies, giving an evident temperature-dependent effect to the static dielectric constant. The polar phonons of PMN give the total contribution to static permittivity about 1000, which corresponds roughly to the dielectric constant in the frequency range of 10–100 GHz [25]. This leads to much higher dielectric constants in the THz region than those in the ultraviolet region [26]. Figure 2 shows the real and imaginary parts of the dielectric functions, which describe the polar-phonon absorption. Figure 2 shows that very high values of permittivity are found at low frequencies, which are below the phonon frequencies. The results from the first-principles calculation of PMN indicate that the high-energy phonon band is not as dispersive compared to the low frequency bands, which can be explained by the band folding due to the ordering of Mg and Nb [7]. Eigenvectors of the mode below 3 THz are important only on Pb, corresponding to low-frequency acoustic antiphase Pb displacements caused by a small diagonal element of the dynamical matrix for Pb. The origin of the mode at 12 THz is puzzling because the first-principles calculations do not show any TO mode near this range [7]. However, the effective medium model on PMN also reproduces this band without assuming any intrinsic TO frequency around 12 THz [21]. This mode is the so-called geometrical resonances (GR), related to the nanoscale polarization inhomogeneity.

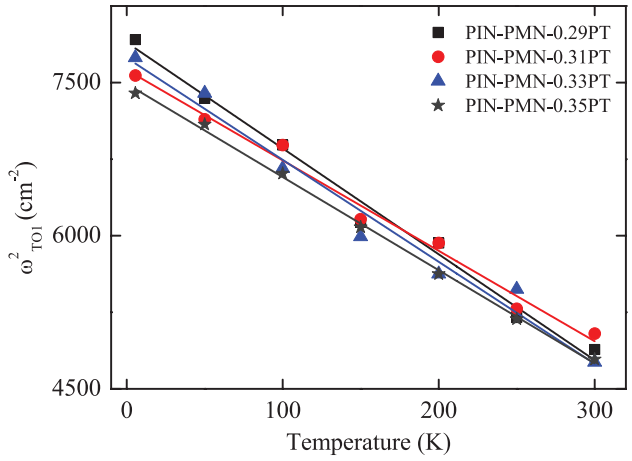

Figure 3. The Cochran law for TO1 modes from PIN-PMN-PT systems.

Table 2. Parameter values of the Cochran fit to TO1 modes for the PIN-PMN-PT crystals.

Crystal	C (cm^2 K^{-1})	T_{cr} (K)
PIN-PMN-0.29PT	10.4 ± 0.5	761 ± 30
PIN-PMN-0.31PT	8.9 ± 0.4	861 ± 36
PIN-PMN-0.33PT	9.9 ± 0.7	775 ± 44
PIN-PMN-0.35PT	9.1 ± 0.2	821 ± 13

It becomes obvious due to a relatively large splitting of the LO2 mode in comparison with its damping, which is a generic feature present in many other relaxors [21].

Most phonon frequencies show softening behavior on heating and the most noticeable softening is shown by the lowest frequency TO1 mode from figure 3. The TO1 phonon splits into A_1 and E components below the Curie temperature, which could be explained by a ferroelectric soft mode within polar clusters [25]. At 5.5 K, the E component is at 0.81 THz while the A_1 component has a higher frequency of 2.67 THz. The symmetry assignments of the A_1 and E modes are straightforward: E modes form the main bands while the A_1 ones are taken as the highest frequency component of each band [21]. The soft mode frequency in PIN-PMN-PT is in good agreement with those in the PMN crystals and films [25]. The TO1 phonon behavior follows the Cochran law $w^2_{TO1} = C(T_{cr} - T)$, where C is the constant and T_{cr} is the critical softening temperature. The fitting parameters are listed in table 2. The parameters are similar to those of PZN-PMN-PSN ceramics, with C from 9.82 to 13.22 cm^2 K^{-1} and T_{cr} from 599 to 849 K [23]. Note that a non-complete softening of the TO1 mode was also found in Pb-based relaxors and ferroelectric $KaTa_{1-x}Nb_xO_3$ [25, 27]. The TO1 soft mode in PMN follows the Cochran law up to 450 K and levels off near 1.5 THz. Above the Burns temperature, it gradually hardens. The soft mode in $KaTa_{1-x}Nb_xO_3$ reaches the minimum at 20 K and again hardens as the temperature further decreases. However, no structural phase transition is revealed in this temperature range. In relaxor ferroelectrics, the main contribution to dielectric constants originates from the dispersion due to polar cluster dynamics below the phonon frequencies.

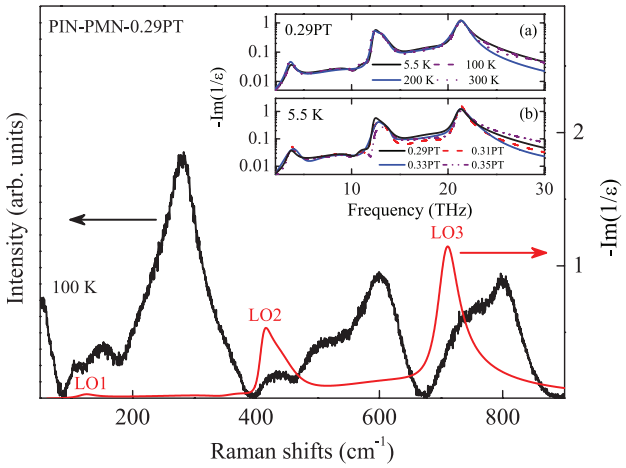

Figure 4. Comparison between Raman spectra and the imaginary part of the inverse permittivity for PIN-PMN-0.29PT crystal at 100 K. The insets (*a*) and (*b*) show the imaginary part of the inverse permittivity of PIN-PMN-0.29PT crystal at selected temperatures and those of PIN-PMN-PT crystals at 5.5 K, respectively.

The damping of the soft mode is 1.8 THz (60 cm^{-1}) at 5.5 K, which indicates that the soft mode is overdamped. This is in agreement with the frequency of the overdamped soft mode in PMN by the INS probe, in which an overdamping soft mode of PMN by the polar nanoregions is observed between 220 K and 620 K [21, 28]. In this case, the frequency of the imaginary parts of permittivity maximum corresponds to v_j^2/γ_j instead of v_j. Most Pb-based perovskites including PMN and PIN show a quenched short-range B-site order. As a result, no superlattice reflections in the x-ray diffraction measurements are shown [25]. However, $Pb(Sc_{1/2}Ta_{1/2})O_3$ shows strong superlattice reflections in x-ray diffraction experiments and the degree of the B-site order can be increased by appropriate annealing [29]. Neutron measurements also exhibit bands near the TO2 mode at 6 THz [28]. The TO mode near 10.3 THz originates mainly from Nb moving opposite to $Mg_{2/3}Mg_{1/3}$-cation and the TO3 mode near 18.5 THz is from $O_{\|}$-($Mg_{2/3}Mg_{1/3}$,Nb) stretching, where $O_{\|}$ is displaced along the B–O bonds. Instability of the Last modes corresponding to Pb–BO_6 stretching vibrations in chemically ordered regions have barriers of the thermal energy order. A highly symmetric array of Mg and Nb ions coordinate Pb ions, showing the softest vibrations. These Pb ions have diagonal Pb-frequencies of about 2.4 THz [7]. The large damping constants are caused by the random fields due to chemical disorder, which can broaden the phonon density of states.

Figure 4 shows the comparison between -Im(1/ε) and Raman spectra. The internal inhomogeneity of the crystals is related to long-wavelength phonons no matter whether they are probed in THz or Raman measurement. Raman shifts have been usually interpreted as the dynamical inhomogeneous depolarization fields, which is from the dynamical charges on the nodal planes of the phonon wave [30]. The scattering geometry, incident photon momentum and momentum conservation condition determine the distance of the nodal planes, which is around a few hundred nanometers.

Both the Raman and IR active modes below the soft mode frequency in the range of 0.75–3 THz reveal antiphase lead displacements that are allowed by the low supercell symmetry [7]. No softening of the TO1 mode is clearly observed in ferroelectric phase transitions. The absence of softening near ferroelectric phase transitions suggests that the transitions are not associated with any changes in the short-range order.

4. Conclusions

In conclusion, the THz spectra and Raman spectra clearly show evidence of polar optical modes splitting in PIN-PMN-PT relaxors. The THz dielectric response of PIN-PMN-PT crystals is divided into three regions corresponding to Axe, Slater and Last-type vibrations, respectively. The Slater band shows an additional weak component, which is related to B-site ordering. The Last-type vibration modes mainly affect the soft mode, describing the homogeneous fluctuations of the order parameter. Dielectric functions, which are extracted by the factorized oscillator model, explain the pseudo-TO mode near 12 THz as a result of nanoscopic heterogeneity. The model is used to express the frequencies of three main polar modes in perovskite relaxors and the A_1–E_1 splitting caused by the underlying polarization.

Acknowledgments

We would like to thank P Chang and K Shi for their technical help. This work was financially supported by the Major State Basic Research Development Program of China (Grant Nos. 2011CB922200 and 2013CB922300), the Natural Science Foundation of China (Grant Nos. 11374097, 61376129 and 61125403), the Projects of Science and Technology Commission of Shanghai Municipality (Grant Nos. 14XD1401500, 13JC1402100, 13JC1404200 and 15YF1413900), the Program for Professor of Special Appointment (Eastern Scholar) at the Shanghai Institutions of Higher Learning and the Project funded by the China Postdoctoral Science Foundation (Grant No. 2014M560357).

References

[1] Scott J F 2007 *Science* **315** 954
[2] Lamela J, Rodenas A, Lifante G Jaque D, Jaque F and Kaminskii A A 2008 *Laser Phys. Lett.* **5** 291
[3] Cross L E 1996 *Mater. Chem. Phys.* **43** 108
[4] Babajanyan V G 2013 *Laser Phys.* **23** 126002
[5] Park S E and Hackenberger W 2002 *Curr. Opin. Solid State Mater. Sci.* **6** 11
[6] Moya X, Kar-Narayan S and Mathur N D 2014 *Nat. Mater.* **13** 439
[7] Prosandeev S A, Cockayne E, Burton B P, Kamba S, Petzelt J, Yuzyuk Y, Katiyar R S and Vakhrushev S B 2004 *Phys. Rev.* B **70** 134110
[8] Zhu J J, Li W W, Xu G S, Jiang K, Hu Z G, Zhu M and Chu J H 2011 *Appl. Phys. Lett.* **98** 091913
[9] Goossens D J 2013 *Acc. Chem. Res.* **46** 2597
[10] Ye Z G 2009 *MRS Bull.* **34** 277
[11] Park S E and Shrout T R 1997 *J. Appl. Phys.* **82** 1804
[12] Noheda B, Cox D E, Shirane G, Park S E, Cross L E and Zhong Z 2001 *Phys. Rev. Lett.* **86** 3891
[13] Noheda B, Cox D E, Shirane G, Gao J and Ye Z G 2002 *Phys. Rev.* B **66** 054104
[14] Zhu J J, Jiang K, Xu G S, Hu Z G, Li Y W, Zhu Z Q and Chu J H 2013 *J. Appl. Phys.* **114** 153508
[15] Kaminskii A A, Lux O, Rhee H, Eichler H J, Yoneda H, Shirakawa A, Ueda K, Ruckamp R, Bohaty L and Becher P 2013 *Laser Phys. Lett.* **10** 073001
[16] Zhang Z, Xiao R, Yang T, Bo X and Wang S 2014 *Laser Phys. Lett.* **11** 035603
[17] Qi T T, Shin Y H, Yeh K L, Nelson K A and Rappe A M 2009 *Phys. Rev. Lett.* **102** 247603
[18] Qi F, Fan S, Notake T, Nawata K, Matsukawa T, Takida Y and Minamide H 2014 *Laser Phys. Lett.* **11** 085403
[19] Ulbricht R, Hendry E, Shan J, Heinz T F and Bonn M 2011 *Rev. Mod. Phys.* **83** 543
[20] Zhu J J, Li W W, Xu G S, Jiang K, Hu Z G and Chu J H 2011 *Acta Mater.* **59** 6684
[21] Hlinka J, Ostapchuk T, Noujni D, Kamba S and Petzelt J 2006 *Phys. Rev. Lett.* **96** 027601
[22] Grinber I and Rappe A M 2004 *Phys. Rev.* B **70** 220101
[23] Macutkevic J, Kamba S, Banys J, Brilingas A, Pashkin A, Petzelt J, Bormanis K and Sternberg A 2006 *Phys. Rev.* B **74** 104106
[24] Bovtun V *et al* 2009 *Phys. Rev.* B **79** 104111
[25] Hlinka J, Petzelt J, Kamba S, Noujni D and Ostapchuk T 2006 *Phase Transit.* **79** 41
[26] Zhu J J, Zhang J Z, Xu G S, Zhang X L, Hu Z G and Chu J H 2014 *Appl. Phys. Lett.* **104** 132903
[27] Chou H, Shapiro S M, Lyons K B, Kjems J and Rytz D 1990 *Phys. Rev.* B **41** 7231
[28] Wakimoto S, Stock C, Birgeneau R J, Ye Z G, Chen W, Buyers W J L, Gehring P M and Shirane G 2002 *Phys. Rev.* B **65** 172105
[29] Reaney I M, Petzelt J, Voitsekhovskii V V, Chu F and Setter N 1994 *J. Appl. Phys.* **76** 2086
[30] Zhang H, Zhou P, Xiao H and Xu X 2014 *Laser Phys. Lett.* **11** 075104